

**Erratum on the paper: "Influence of a Feshbach resonance on the photoassociation of LiCs", New Journal of Physics, vol. 11, p.055034 (2009).**

**J Deiglmayr, A Grochola, M Repp, R Wester, M Weidemüller<sup>‡</sup>,**

Physikalisches Institut, Albert-Ludwigs-Universität Freiburg, Germany

**O Dulieu,**

Laboratoire Aimé Cotton, CNRS, University Paris-Sud XI, Orsay, France

**P Pellegrini and R Côté**

Department of Physics, University of Connecticut, Storrs, USA

**Abstract.** Erratum on the paper: "Influence of a Feshbach resonance on the photoassociation of LiCs", New Journal of Physics, vol. 11, p.055034 (2009).

PACS numbers: 37.10.Mn, 33.20.-t, 33.80.Rv

<sup>‡</sup>

E-mail: weidemueller@physi.uni-heidelberg.de

In the paper by Deiglmayr *et al* [1], we found a sign error in the transformation of the scattering wave function between the atomic basis (eq. 6) and the molecular basis (eq. 7) that we used for the case  $m_F = 5$  for the following atomic state:

$$\begin{aligned}
 &|f_1 = 2, m_{f_1} = 2, f_2 = 3, m_{f_2} = 3\rangle = \\
 &+ \sqrt{\frac{7}{16}}|S = 0, m_S = 0, I = 5, m_I = 5\rangle \\
 &+ \sqrt{\frac{7}{16}}|S = 1, m_S = 0, I = 5, m_I = 5\rangle \\
 &- \sqrt{\frac{3}{80}}|S = 1, m_S = 1, I = 4, m_I = 4\rangle \\
 &- \sqrt{\frac{7}{80}}|S = 1, m_S = 1, I = 5, m_I = 4\rangle
 \end{aligned}$$

In consequence, the results of the left column of Fig. 5 of the quoted paper are correct, while those of the right column are not. The corrected figure is now displayed in Figure 1 below. In particular there is not anymore influence of the triplet part of the wave function on the singlet one (see upper panel of the right column). This affects also Figures 6 and 7 of reference [1]. The black trace of the upper part of Figure 6 is wrong, as well as the results of Figure 7.

The main consequence concerns the interpretation of the experimental results reported in Figure 8 of Deiglmayr *et al* [1]. The magnitude and modulation of the photoassociation (PA) rate observed in the experiment can be interpreted only if the triplet component of the scattering wave function is involved, as it was discussed in the paper. However, the model employed in reference [1] cannot reproduce these results.

The role of the triplet component of the scattering wave function can be invoked in the PA towards the  $B^1\Pi$  levels by considering the small spin-orbit coupling of the  $B^1\Pi$  state with the neighboring triplet states (see Figure 4 of Deiglmayr *et al* [1]), while the modulations of the PA rate may be influenced by a slight variation of the scattering length of the lowest  $a^3\Sigma^+$  state. These issues will be considered in a future paper.

We would like to thank Prof. E. Tiemann for pointing out to us this error sign.

[1] J. Deiglmayr, P. Pellegrini, A. Grochola, M. Repp, R. Côté, O. Dulieu, R. Wester, and M. Weidemüller. Influence of a feshbach resonance on the photoassociation of lics. *New J. Phys.*, 11:055034 (2009).

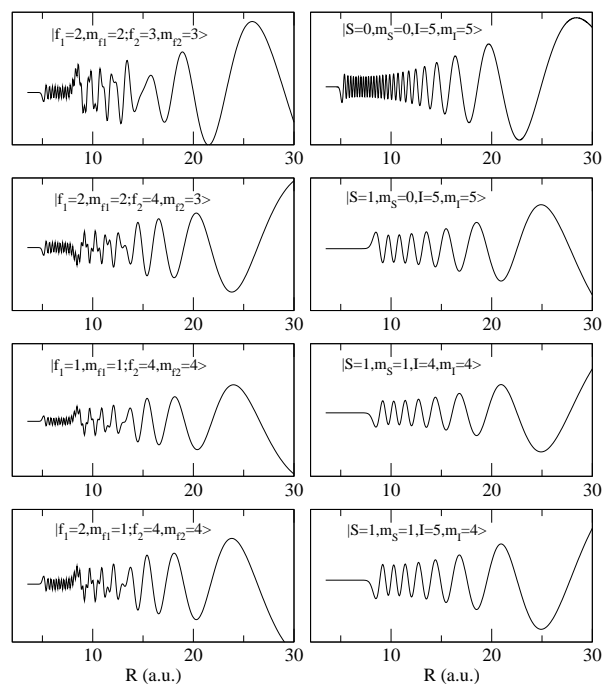


**Figure 1.** Components of the energy-normalized radial wave function for a LiCs pair colliding at 500  $\mu\text{K}$ , in the atomic basis (left column) and in the molecular basis (right column). The displayed case corresponds to  $m_{f_1} + m_{f_2} = 5$ . Under the given experimental conditions, the upper-most atomic state  $f_1 = 2$ ,  $m_{f_1} = 2$ ,  $f_2 = 3$ ,  $m_{f_2} = 3$  is the only open entrance channel, the three other shown states are closed channels. Note that there is no line-to-line relation between the states listed in each column.

# Influence of a Feshbach resonance on the photoassociation of LiCs

J Deiglmayr<sup>1,2</sup>, P Pellegrini<sup>3</sup>, A Grochola<sup>4</sup>, M Repp<sup>1</sup>, R Côté<sup>3</sup>, O Dulieu<sup>2</sup>, R Wester<sup>4</sup> and M Weidemüller<sup>1</sup>

<sup>1</sup> Physikalisches Institut, Ruprecht-Karls-Universität Heidelberg, Germany

<sup>2</sup> Laboratoire Aimé Cotton, CNRS, Université Paris-Sud XI, Orsay, France

<sup>3</sup> Department of Physics, University of Connecticut, Storrs, USA

<sup>4</sup> Physikalisches Institut, Albert-Ludwigs-Universität Freiburg, Germany

E-mail: weidemueller@physi.uni-heidelberg.de,  
olivier.dulieu@lac.u-psud.fr and rcote@phys.uconn.edu

**Abstract.** We analyse the formation of ultracold  ${}^7\text{Li}{}^{133}\text{Cs}$  molecules in the rovibrational ground state through photoassociation into the  $B^1\Pi$  state, which has recently been reported [J. Deiglmayr *et al.*, Phys. Rev. Lett. **101**, 133004 (2008)]. Absolute rate constants for photoassociation at large detunings from the atomic asymptote are determined and are found to be surprisingly large. The photoassociation process is modeled using a full coupled-channel calculation for the continuum state, taking all relevant hyperfine states into account. The enhancement of the photoassociation rate is found to be caused by an “echo” of the triplet component in the singlet component of the scattering wave function at the inner turning point of the lowest triplet  $a^3\Sigma^+$  potential. This perturbation can be ascribed to the existence of a broad Feshbach resonance at low scattering energies. Our results elucidate the important role of couplings in the scattering wave function for the formation of deeply bound ground state molecules via photoassociation.

PACS numbers: 33.20.-t, 33.80.Rv, 34.50.Rk, 37.10.Mn, 67.85.-d

Submitted to: *New J. Phys.*

## 1. Introduction

The formation and manipulation of molecules at ultralow temperatures has undergone tremendous progress in the past years [1, 2]. The ‘holy grail’ of the field is the creation of a stable quantum-degenerate gas of molecules, in which all molecules populate the ground state of the system, comprising motional and internal degrees of freedom. Such a system provides exquisite possibilities for further control and may thus serve as the starting point to investigate future applications of ultracold molecules such as precision measurements of fundamental constants [3] and ultracold chemical reactions [4]. Dipolar molecules are of particular interest in this context, as the dipolar interaction can be exploited for the study of quantum many-body phenomena [5, 6] or the realization of various schemes for quantum information processing [7, 8, 9, 10]. The most promising path towards the goal of a quantum-degenerate gas of molecules in the internal ground state consists in the association of ultracold atoms, either by magnetic or oscillatory electric fields. In the first case, called magnetoassociation, the molecules are formed through a magnetically induced Feshbach resonance coupling the free pair of atoms to a weakly bound molecular state. The transfer into the absolute internal ground state can then be accomplished by stimulated rapid adiabatic passage (STIRAP) in a combination of pulsed laser fields. This scheme has recently been successfully applied to form deeply bound molecules of Rb<sub>2</sub> [11], Cs<sub>2</sub> [12, 13], and KRb [14]. The other, closely related approach consists of the direct photoassociation of molecules out of an ultracold gas followed by spontaneous emission, which may be followed by a second bound-bound excitation step to transfer the molecules into the vibrational ground state. This method has led to the formation of the vibrational ground state of K<sub>2</sub> [15], RbCs [16], Cs<sub>2</sub> [17], and LiCs [18]. Magnetoassociation combined with STIRAP has the great advantage of being a fully coherent process which preserves the phase-space density of the initial gas, while photoassociation followed by spontaneous emission leads to smaller phase-space densities but can be driven as a continuous process thus allowing for the steady accumulation of molecules, e.g. in an optical or static trap. Concerning ultracold dipolar gases we note that among the above listed ultracold molecules in the ground state the only dipolar ones are the heteronuclear molecules RbCs, KRb, and LiCs. They all possess significant dipole moments of 1.2 [19], 0.57 [14], and 5.5 Debye [19] respectively.

Here we focus on a recent experiment on the formation of ultracold bosonic <sup>7</sup>Li<sup>133</sup>Cs ground state molecules with low vibrational and rotational quantum numbers [18, 20]. The molecule formation consists in a particularly simple two-step photoassociation (PA) procedure comprising the laser excitation of the  $B^1\Pi$  state out of an ultracold mixture of lithium and cesium atoms. The vibrational state  $v'=4$  of this electronically excited state has a particularly large Franck-Condon overlap with the vibrational level  $v''=0$  of the ground state  $X^1\Sigma^+$  which leads to a measurable population of this lowest vibrational level by spontaneous emission. As only low angular momenta are involved due to the ultralow temperature, ultracold molecules in the rovibrational ground state could be detected. The rate limiting process of this PA scheme was the excitation of the tightly bound  $B^1\Pi(v'=4)$  level out of the dilute gas. Actually, the observation of PA of molecules in this state at short internuclear distance came as a surprise, as naive estimates delivered negligible formation rates. In this article, we investigate the PA process in more detail. We find that the PA rate is strongly enhanced by an increased amplitude of the scattering wave function at short internuclear distances. It is important to note that despite the presence of spin-orbit

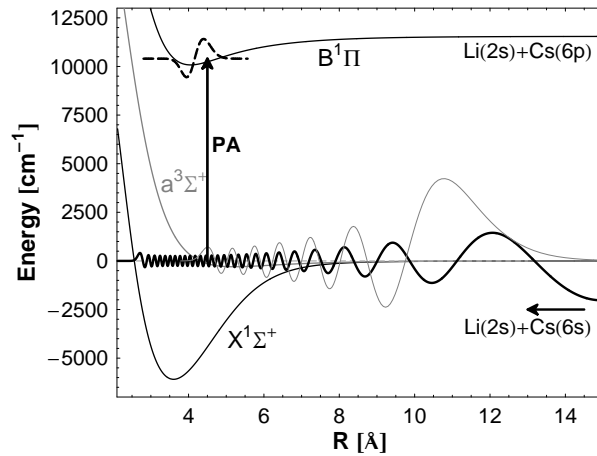


**Figure 1.** Schematic view of the photoassociation process at short internuclear distances: the component of the scattering wave function related to the singlet potential  $X^1\Sigma^+$  (solid black line) is coupled around the inner turning point of the triplet potential  $a^3\Sigma^+$  to a level in the excited singlet state  $B^1\Pi$  (black dashed line). A typical bound state wave function in the  $a^3\Sigma^+$  potential is also shown (gray line).

coupling close to the atomic asymptote, for deeply bound levels the excited state has very pure singlet character. Therefore only the singlet component of the scattering wave function is relevant for the PA rate. Figure 1 depicts this situation: the Franck-Condon overlap between the scattering wave function in the singlet potential  $X^1\Sigma^+$  and low lying levels in the  $B^1\Pi$  potential vanishes, as the fast oscillations of the scattering wave function at short internuclear distances average to zero. However, experimentally we observe high PA rates into excited levels, which correspond to a transition around the inner turning point of the  $a^3\Sigma^+$  state. Therefore we conclude that the scattering wave function is locally perturbed by the presence of a bound level with strong triplet character, indicating the proximity of a Feshbach resonance. Indeed the importance of closed coupled channels for the scattering wave function close to a Feshbach resonance has recently been theoretically explored by some of us as a means to strongly enhance the PA formation rate of ultracold molecules [21]. The perturbation introduced by this Feshbach resonance leads to an “echo” of the triplet-like wave function on the singlet component of the scattering wave function, which increases the Franck-Condon overlap between the scattering wave function and tightly bound levels in the  $B^1\Pi$  potential. We present a model containing an accurate and complete description of the continuum scattering wave function and of the excited molecular wave function, which proves the validity of this picture and reproduces the experimental observations accurately.

The paper is organized as follows: In section 2 we describe our experiment on the formation and detection of ultracold LiCs molecules in low vibrational and rotational states of the singlet ground state. Section 3 is then devoted to a quantitative analysis of measured line strengths and rate constants for PA into the  $B^1\Pi$  state. In section 4 we develop the theoretical model: A brief overview is given on how PA rates are computed based on wave functions of the excited levels. It is explained, how hyperfine

interactions in the scattering entrance channel couple singlet and triplet components and lead to an “echo” of triplet features in the singlet component of the scattering wave function. Numerical methods are introduced, and the results obtained by the coupled-channel calculation are discussed. Results for the coupled and uncoupled cases are compared with the experimental findings. Section 5 discusses the results of the paper.

## 2. Formation and detection of ultracold LiCs molecules

Details of the experimental setup for the formation and detection of ultracold LiCs molecules have already been described in detail in Refs. [18, 20, 22]. Therefore, we will confine ourselves to the description of the main experimental features.  $4 \times 10^7$   $^{133}\text{Cs}$  atoms and  $10^8$   $^7\text{Li}$  atoms are trapped in overlapped magneto-optical traps (MOT’s) at densities of  $3 \times 10^9 \text{ cm}^{-3}$  and  $10^{10} \text{ cm}^{-3}$  respectively. The MOT for cesium is realized as a dark spontaneous force optical trap [23], in which the atoms are kept most of the time (typically 97%) in the dark lower hyperfine ground state leading to higher densities and to a reduction of inelastic collisions. In the conventional lithium MOT, most of the atoms populate the upper hyperfine ground state (>80%). Lithium and cesium atoms therefore collide mainly on the  $\text{Li}(2^2\text{S}_{1/2}, f=2) + \text{Cs}(6^2\text{S}_{1/2}, f=3)$  asymptote. We measure a cesium temperature of  $250(50)\mu\text{K}$  using time-of-flight expansion and deduce a lithium temperature of  $600(150)\mu\text{K}$  by fitting the line shape of a narrow PA resonance [20] to the model of reference [24]. In the center-of-mass frame, this corresponds to a mean collision energy of  $580(80)\mu\text{K}$ .

In PA, a colliding pair of atoms absorbs a photon resonant to a transition into a bound excited molecular level [25, 26]. For this process we use up to 500 mW of light from a tunable Ti:Sa laser. The beam is collimated to a waist of 1.0 mm and continuously illuminates the two overlapped atom traps. The excited molecules decay within a few tens of nanoseconds either into bound ground state molecules or back into free pairs of atoms with additional kinetic energy [27]. For the detection of ground state molecules, we use a pulsed dye laser with a repetition rate of 20 Hz (typical pulse energy 8 mJ, beam diameter  $\sim 5$  mm). Molecules in the ground state are ionized by resonant-enhanced multi-photon ionization (REMPI), in our case by two photons of the same color. The resulting  $\text{LiCs}^+$  ions are then separated from a background of  $\text{Cs}^+$  ions in a time-of-flight mass spectrometer and are finally detected using a micro-channel plate and single-ion-counting electronics. Figure 2 (a) depicts the states involved in the formation and detection of ground state molecules. Exemplary PA resonances are shown in figure 2 (b).

We focus on the  $B^1\Pi$  state of LiCs, which has been studied previously in a heat-pipe with high-resolution laser-induced fluorescence spectroscopy [28]. Due to spin-orbit interaction, this state is asymptotically correlated to  $\text{Li}(2^2\text{S}_{1/2}) + \text{Cs}(6^2\text{P}_{3/2})$  after its coupling with neighboring triplet states. For convenience, we will refer to it as the  $B^1\Pi$  state. Additionally to the vibrational levels  $v' = 0 - 25$  identified in reference [28], we found vibrational levels  $v' = 26 - 35$ , where the last level  $v' = 35$  is bound only by a few GHz. For most lines, we observe rotational components  $J' = 1$  and  $J' = 2$ , which are split into several hyperfine sub-lines. The typical overall width of these hyperfine structures ranges for  $J' = 1$  resonances from 550 MHz for low vibrational levels to 900 MHz for the last bound levels, while the  $J' = 2$  resonances are narrower, ranging from a width of 300 MHz for low  $v'$ s to 600 MHz close to the asymptote.

We detect PA resonances by ionizing ground state molecules produced after

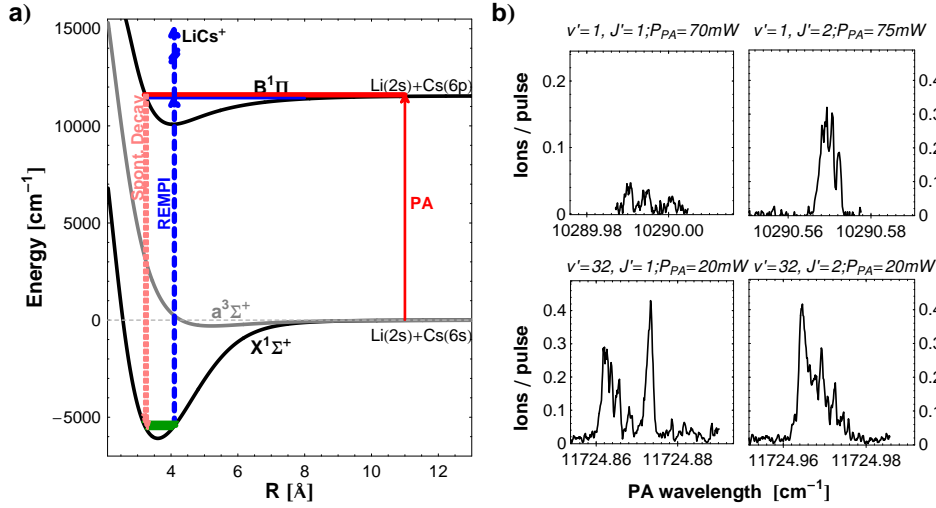


**Figure 2.** (a) Photoassociation and detection scheme together with the relevant levels of LiCs: after PA into levels of the  $B^1\Pi$  state, molecules decay spontaneously into  $X^1\Sigma^+$  molecules. These molecules are ionized by two photons, where resonant intermediate states enhance the ionization rate. (b) Exemplary photoassociation resonances for deeply bound levels ( $v'=1$ ) and levels close to the asymptote ( $v'=31$ ) (detected at different REMPI wavelengths, see text).

spontaneous decay from the photoassociated, electronically excited molecules. Three different frequencies were used for the ionization of these ground state molecules. Molecules produced by PA in low vibrational states  $v' < 9$  are ionized at  $16999.7 \text{ cm}^{-1}$ , where three resonant transitions for the first step,  $X^1\Sigma^+, v''=0 \rightarrow B^1\Pi, v'=14$ ,  $X^1\Sigma^+, v''=1 \rightarrow B^1\Pi, v'=18$ , and  $X^1\Sigma^+, v''=2 \rightarrow B^1\Pi, v'=23$ , are nearly degenerate [20]. Ground state molecules formed after PA via intermediate vibrational levels  $v' \geq 9$  and  $v' \leq 15$  are detected at  $16859.4 \text{ cm}^{-1}$ , a REMPI resonance where a strong contribution from the transition  $X^1\Sigma^+, v''=2 \rightarrow B^1\Pi, v'=19$  was identified [20]. While the here identified ground state levels make up for an important part of the observed ion signal, molecules in other ground state levels might also be ionized by the given laser frequency via intermediate states other than  $B^1\Pi$ . Molecules which have decayed from high lying vibrational levels  $v' > 15$  are all ionized at  $14692.7 \text{ cm}^{-1}$ . The ionization process at this resonance has not yet been analysed. However, it is very likely that high lying levels in the electronic ground state  $X^1\Sigma^+$  are ionized at this energy through a broad band of levels in different electronic states between the asymptotes  $\text{Li}(2^2S_{1/2}) + \text{Cs}(6^2P_{3/2})$  and  $\text{Li}(2^2S_{1/2}) + \text{Cs}(5^2D_{3/2})$ .



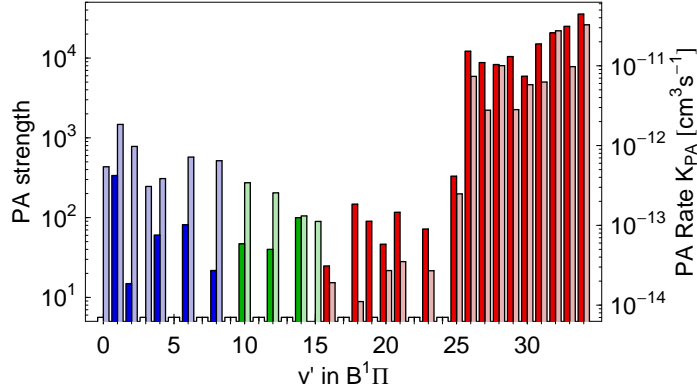


**Figure 3.** Photoassociation line strength (given as number of molecules $\times$ MHz/s/mW) and PA rates of all observed levels  $v'$ ,  $J'=1$  (left, dark colors) and  $J'=2$  (right, light colors) in the  $B^1\Pi$  state. The PA resonances are integrated and normalized to the PA laser power. Absolute rates are given for a reference PA intensity of  $30\text{W}/\text{cm}^2$ . Ionization wavelengths used for detection are  $14692.7\text{cm}^{-1}$  (red),  $16859.4\text{cm}^{-1}$  (green), and  $16999.7\text{cm}^{-1}$  (blue), respectively.

### 3. Line strengths of the photoassociation resonances and formation rate constants

#### 3.1. Photoassociation resonance line strengths

The strength of the PA resonances are shown in figure 3 for all observed  $v'$ ,  $J'=1$  and  $J'=2$  levels. The last bound level  $v'=35$  was excluded from the analysis, as the cesium MOT is strongly perturbed by the PA laser at small detunings from the atomic asymptote. In order to reduce the influence of the varying hyperfine structure, the full PA spectrum is background-subtracted and integrated for each ro-vibrational level, therefore summing up the contributions from all hyperfine components. In order to directly compare the line strength of PA resonances measured under different experimental conditions, the integrated peak area is normalized to the intensity of both the PA laser and the ionization laser. At a strong line we confirmed for both the PA and the REMPI step that the molecule formation rate is indeed linear in both intensities. For the two-photon ionization, this indicates that the first resonant-enhanced transition is strongly saturated and therefore the probability for this transition does not depend on the intensity of the ionization laser above a certain, not determined threshold. The PA laser intensities were chosen for each resonance in such a way that the maximum count rate does not exceed 0.5 ions/pulse to avoid saturation of the single ion detection.

One uncertainty remains, which limits the comparability between different PA resonances. As discussed in Sect. 2, we do not detect the excited molecules directly but only the ground state molecules formed after spontaneous decay. As the Frank-Condon factors between excited state and ground state levels vary with the PA level  $v'$ , also the distribution of populated ground state levels after spontaneous decay depends on the PA level [20]. These differences in the populated levels can lead to

variations in the overall ionization efficiency for molecules produced at different PA resonances. It is difficult to estimate the influence of this varying detection efficiency on the measured PA strengths, as many off-resonant and nonlinear processes play a role in the REMPI ionization scheme. We observe however that the calculated ground state distributions vary only slowly with the excited level  $v'$ . Also from measurements of the same PA line at different ionization resonances, we deduce that this variation does not exceed a factor of ten over neighboring vibrational levels. Nonetheless this constitutes one of the main uncertainties in the reported PA rate constants. For levels close to the asymptote we also compare the molecule formation rate deduced from the ion signal with measurements of trap loss. We find fair agreement within one order of magnitude, which is acceptable in view of the large systematic uncertainty on the efficiency of the ion detection.

### 3.2. Absolute molecule formation rates

In order to relate the PA line strengths to the formation rate of molecules, we further analyse the detection efficiency for ground state molecules. As the formed molecules are not trapped, they leave the ionization region some time after their production due to their thermal velocity of roughly  $300 \mu\text{K}$  (calculated from the velocities of the atomic constituents) and acceleration due to gravity. Taking the size and the alignment of the ionization beam (roughly one beam diameter below the trapped atom clouds) into account, we estimate a geometric overlap factor of 40%. Therefore, only 40% of the formed molecules have a chance to be ionized. Assuming that the first bound-bound transition during the ionization of ground state molecules is on resonance and thus fully saturated, we use a typical ionization cross section of  $10^{-18} \text{cm}^2$  [29] to approximate the ionization probability  $p_{\text{ion}}$  for pulse energies  $E_{\text{REMPI}}$  of up to few tens of mJ by  $p_{\text{ion}} \simeq 8 \times 10^{-3} E_{\text{REMPI}}$  where  $E_{\text{REMPI}}$  is measured in mJ. Finally the detector efficiency is around 20% [30], leading to an overall efficiency of the detection setup on the order of  $10^{-3}$  for typical experimental parameters. By averaging over many cycles (typically around 100), even very weak PA resonances can be detected.

The rate constant  $K_{\text{PA}}$  for the PA process is calculated by first linearly scaling the number of produced molecules per second to a reference PA intensity (chosen to be  $30 \text{ W/cm}^2$ ) yielding a molecular formation rate  $k$ . In our experimental geometry the diameter of the PA laser beam and of the lithium MOT are both larger than the size of the cesium MOT. The rate coefficient  $K_{\text{PA}}$  is then simply given by  $K_{\text{PA}} = k/n_{\text{Li}}/N_{\text{Cs}}$  with the peak lithium density  $n_{\text{Li}}$  and the cesium particle number  $N_{\text{Cs}}$ . The measured rate coefficients are shown in figure 3 (right axis). For the last bound states we observe PA rate constants on the order of  $4 \times 10^{-11} \text{cm}^3/\text{s}$ . These are of the same order of magnitude as the rate constants observed in the PA of  $\text{Cs}_2$  [31, 32] and  $\text{KRb}$  [33], as was predicted by Azizi *et al.* [34].

The PA rate decreases towards lower vibrational states, which are excited at shorter internuclear distance corresponding to lower pair density. Below  $v' = 25$  we observe a change towards a distinct oscillatory pattern in the rate constants. While some vibrational levels show rate constants varying by no more than one order of magnitude, adjacent levels are below the detection threshold of our setup. For very deeply bound levels  $v' \leq 6$  the PA rate appears to increase again, *e.g.* for the  $v'=1, J'=1$  level at a detuning of more than  $1.400 \text{ cm}^{-1}$  we measure a PA rate coefficient on the order of  $4 \times 10^{-13} \text{cm}^3/\text{s}$ . This is unexpectedly high, as a single channel scattering calculation predicts a rate constant below  $10^{-19} \text{cm}^3/\text{s}$  due to the low Franck-Condon

overlap between the rapidly oscillating singlet scattering wave function and the excited state wave function at short internuclear distances. In the following, we describe the theoretical framework employed to explain the unexpectedly large formation rate in the singlet electronic state.

#### 4. Model of photoassociation into the $B^1\Pi$ electronic state

##### 4.1. Theoretical photoassociation rates

A PA rate  $K_{\text{PA}}^{v'} = \langle v_{\text{rel}} \sigma_{\text{PA}}^{v'} \rangle$  from an initial scattering continuum state to an excited vibrational level  $v'$  is obtained using the cross section  $\sigma_{\text{PA}}^{v'}$  of two atoms colliding in the presence of a laser field, and averaged over the relative velocity distribution  $v_{\text{rel}}$ . For a thermal atomic gas, a Maxwell-Boltzmann distribution characterized by a temperature  $T$  is appropriate, and assuming a PA laser beam of negligible linewidth and resonant for the transition to  $v'$ , we have [35]:

$$K_{\text{PA}}^{v'}(T, I) = \frac{1}{hQ_T} \int_0^\infty d\varepsilon e^{-\varepsilon/k_B T} \frac{\gamma_{v'} \gamma_s}{\varepsilon^2 + (\frac{\gamma_{v'} + \gamma_s}{2})^2}, \quad (1)$$

where  $Q_T = (2\pi\mu k_B T/h^2)^{3/2}$ ,  $h$  and  $k_B$  are the Planck and Boltzmann constant, respectively,  $\varepsilon = \mu v_{\text{rel}}^2/2$  is the relative kinetic energy of the colliding pair of atoms of reduced mass  $\mu$ , and  $\gamma_{v'}$  is the natural linewidth of the photoassociated level.

Using Fermi's Golden Rule, we obtain an expression for the stimulated emission width  $\gamma_s$  in terms of the initial scattering state  $\Psi_{\varepsilon, \ell}$  at energy  $\varepsilon$ , and the excited vibrational state  $\phi_{v', J'}$

$$\gamma_s = \frac{\pi I}{\epsilon_0 c} |\langle \phi_{v', J'} | D(R) | \Psi_{\varepsilon, \ell} \rangle|^2. \quad (2)$$

Here,  $\ell$  labels the partial wave,  $I$  is the intensity of the PA laser, and  $\epsilon_0$  and  $c$  are the vacuum permittivity and speed of light, respectively. We will restrict ourselves to  $s$ -wave scattering in the entrance channel, and thus set  $\ell=0$ . This is well justified, as the measured relative temperature in the experiment of 580  $\mu\text{K}$  is well below the  $p$ -wave barrier height of 1.6 mK.

We obtain the scattering wave function in the entrance channel  $\Psi_{\varepsilon, \ell}$  by solving the Hamiltonian of two colliding atoms with hyperfine interactions, which mix the singlet  $X^1\Sigma^+$  and triplet  $a^3\Sigma^+$  states. In addition to this scattering wave function and the wavefunction of the excited level  $\phi_{v', J'}$  (see descriptions in the next sections), we need the dipole transition moment  $D(R)$  to calculate  $\gamma_s$ . Its  $R$ -dependent form is calculated using the theoretical method and parameters described in reference [19]. The value of the dipole moment does not vary by more than 10% around a mean value of 4.0 a.u. over the relevant range of distances.

##### 4.2. Excited state vibrational wave functions

PA is performed to the excited  $B^1\Pi$  molecular potential. High resolution spectroscopy of this potential has been published in reference [28]. We use a potential fitted to the levels observed in this work combined with the additional levels observed by us [36]. However, we note that the spin-orbit coupling of the  $B^1\Pi$ ,  $b^3\Pi$ , and  $c^3\Sigma^+$  states becomes important near the dissociation limit and cannot be neglected. The Hund's case (a) is therefore no longer valid and the  $B^1\Pi$  state should be treated as  $\Omega=1$  in Hund's case (c). To estimate the strength of the singlet-triplet mixing we used a simple

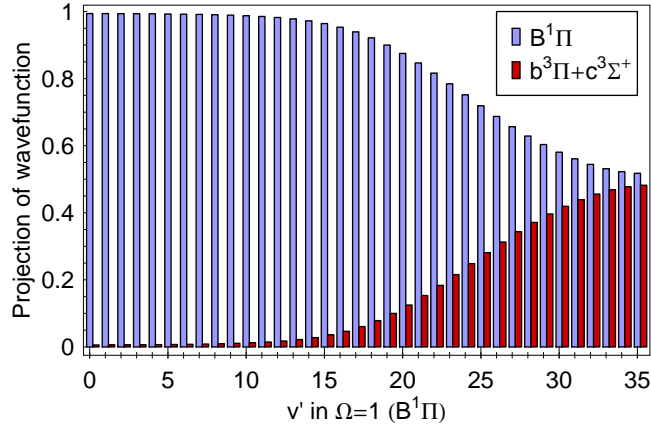


**Figure 4.** Projection of the  $\Omega=1$  ( $B^1\Pi$ ) wave functions onto the singlet component  $B^1\Pi$  (light blue) and the triplet components  $b^3\Pi$  and  $c^3\Sigma^+$  (dark red). At low  $v$ 's the state can therefore be identified as pure  $B^1\Pi$ , while for  $v'\sim 20$  and higher the triplet character, induced by spin-orbit coupling, becomes important.

3-channel model [37], coupling ab-initio curves for  $B^1\Pi$ ,  $b^3\Pi$ , and  $c^3\Sigma^+$  (calculated as described in reference [19]) with constants proportional to the atomic finestructure interaction of  $554.04\text{ cm}^{-1}$  [38, 39] for the first asymptote of cesium. Wave functions and projections on the three channels were calculated using the mapped Fourier grid method [40].

As can be seen in figure 4, the components of the  $\Omega=1$  ( $B^1\Pi$ ) wave function related to the coupled triplet states become sizable above  $v' = 20$ . For the highest lying levels, the summed amplitude of these components reaches nearly 50%. This value can be taken as a first estimate for the influence of the excited state mixing on the PA line strength: the triplet component of the excited state can now be populated from the triplet component of the scattering state. In general (*i.e.* as long as there are no strong local perturbations of the wave functions), the excited triplet components will only decay into triplet ground state molecules or free pairs of atoms, so they will not contribute to the production of deeply bound singlet molecules. In such a case one would expect for high lying levels to observe PA rates, which are reduced by the amount of the triplet projection shown in figure 4 when compared to PA rates derived from the here presented theory. However, since the focus of this work is on the lowest vibrational levels (below  $v' = 20$ ), we treated the excited potential as a pure  $B^1\Pi$  state in our calculation.

#### 4.3. Scattering wave function of the ground state

If we label  $\vec{s}_j$  and  $\vec{i}_j$  the electronic and nuclear spin for the atom  $j$ , respectively, then the total spin  $f_j$  of atom  $j$  (with projection  $m_{f_j}$ ) is given by  $\vec{f}_j = \vec{s}_j + \vec{i}_j$ . The total angular momentum without rotation is  $\vec{F} = \vec{f}_1 + \vec{f}_2$ . The two-body hyperfine Hamiltonian for atoms of relative momentum  $\vec{p}$  (and reduced mass  $\mu$ ) can be written

as

$$H = \frac{p^2}{2\mu} + \sum_{j=1}^2 \frac{a_{\text{hf}}^{(j)}}{\hbar^2} \vec{s}_j \cdot \vec{i}_j + V^c, \quad (3)$$

where  $V^c$  is the potential energy operator, and  $a_{\text{hf}}^{(j)}$  is the hyperfine constant for atom  $j$ . No spin-rotation coupling is introduced here, which means that the rotational angular momentum  $\ell$  is fixed.  $V^c$  can be expressed in terms of the singlet  $V_0(R)$  and triplet  $V_1(R)$  molecular potentials using the projection operators  $P^0$  and  $P^1$ :

$$V^c = V_0(R)P^0 + V_1(R)P^1. \quad (4)$$

As it is the case for the excited  $B^1\Pi$  state, the ground electronic singlet and triplet potentials are known from high resolution spectroscopy [41]. We used the potential curves as given in the reference, with a cubic spline interpolation of the given pointwise representation connected to the given long-range expansion.

The hyperfine Hamiltonian in Eq.(3) only couples hyperfine channels with the same total angular momentum projection  $m_F = m_{f_1} + m_{f_2}$ . For  ${}^7\text{Li}$  with  $i_1 = 3/2$  and  ${}^{133}\text{Cs}$  with  $i_2 = 7/2$  (both with  $s_1 = s_2 = 1/2$ ),  $m_F$  takes values from -6 to +6, leading to a total degeneracy of the atom pair of 128. However, atoms mainly collide on the  $\text{Li}(2^2S_{1/2}, f = 2) + \text{Cs}(6^2S_{1/2}, f = 3)$  asymptote, and thus only 35 degenerate entrance channels have to be considered.

The hyperfine Hamiltonian (3) is expressed and diagonalized in the atomic basis

$$|f_1, m_1; f_2, m_2\rangle \equiv |f_1, m_1\rangle_{\text{Li}} \otimes |f_2, m_2\rangle_{\text{Cs}}, \quad (5)$$

and the total collisional wave function is then expressed as

$$|\Psi_{\epsilon, \ell}\rangle = \sum_{\alpha=1}^N \psi_{\alpha}(R) \{|f_1, m_1\rangle \otimes |f_2, m_2\rangle\}_{\alpha}, \quad (6)$$

where  $\alpha$  labels a particular channel, and  $N$  is the number of coupled hyperfine channels which depends on the value of  $m_F$ . Here,  $\psi_{\alpha}(R)$  is the radial wave function of channel  $\alpha$ .

For the calculation of the Franck-Condon factors, only the singlet component of the total collisional wave function is relevant. A rotation is thus performed to express the wave function in the molecular basis  $|S, m_S, I, m_I\rangle$  with  $\vec{S} = \vec{s}_1 + \vec{s}_2$  and  $\vec{I} = \vec{i}_1 + \vec{i}_2$ . We then have

$$|\Psi_{\epsilon, \ell}\rangle = \sum_{\beta=1}^N \phi_{\beta}(R) \{|S, m_S, I, m_I\rangle\}_{\beta}, \quad (7)$$

where  $\phi_{\beta}(R)$  is the wave function in this basis (with  $N$  channels  $\beta$ ). We can go from one basis to another basis using angular momentum algebra.

#### 4.4. Results for $m_F = 5$ scattering state

For simplicity we concentrate here on the particular case of  $m_F = 5$ , corresponding to the coupling of the four channels listed in Table 1 by the hyperfine interaction. These four states represent approximately 1/10th of a total of 35 degenerate channels of the entrance channel. In order to compute the dipole transition matrix elements  $\langle \phi_{v', J'} | D(R) | \Psi_{\epsilon, \ell} \rangle$  appearing in Eq.(2) for  $\gamma_s$ , the wave functions are needed: the Schrödinger equation is solved with the Mapped Fourier Grid Hamiltonian (MFGH) method [40, 21]. All calculations are performed at a collision energy of 500  $\mu\text{K}$ : No

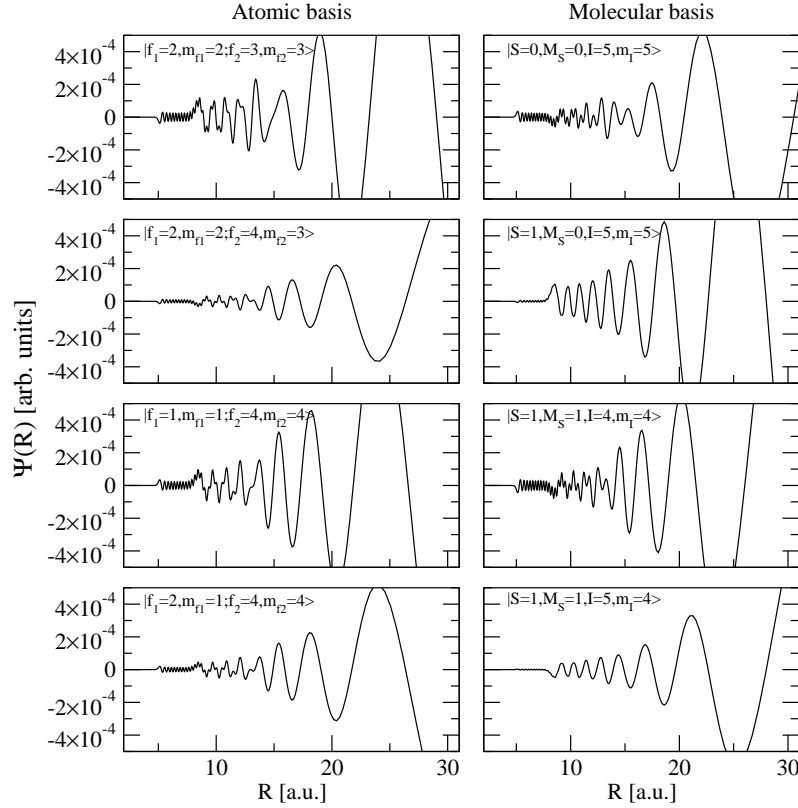


**Figure 5.** Components of the energy-normalized radial wave function for a Li-Cs pair colliding at 500  $\mu\text{K}$ , in the atomic basis (left columns) and in the molecular basis (right column). Under the given experimental conditions, the upper-most atomic state  $f_1=2, m_{f_1}=2, f_2=3, m_{f_2}=3$  is the only open entrance channel, the three other shown states are closed channels. Note that there is no line-to-line relation between the states listed in each column.

large variations of the results are expected for slightly varying collision energies, so the experimental collision energy is very well approximated by this value. The components of the initial radial wave function are drawn in figure 5 in the atomic (left column) and molecular (right column) basis. It is striking to see in both columns that, in contrast

	Atomic basis	Molecular basis
$m_F = 5$	$f_1 = 2, m_{f_1} = 2, f_2 = 3, m_{f_2} = 3$	$S = 0, m_S = 0, I = 5, m_I = 5$
	$f_1 = 2, m_{f_1} = 2, f_2 = 4, m_{f_2} = 3$	$S = 1, m_S = 0, I = 5, m_I = 5$
	$f_1 = 1, m_{f_1} = 1, f_2 = 4, m_{f_2} = 4$	$S = 1, m_S = 1, I = 4, m_I = 4$
	$f_1 = 2, m_{f_1} = 1, f_2 = 4, m_{f_2} = 4$	$S = 1, m_S = 1, I = 5, m_I = 4$

**Table 1.** Values for the quantum numbers of the collisional channels of the  $m_F = 5$  subspace for the atomic basis  $|f_1, m_{f_1}, f_2, m_{f_2}\rangle$  and the molecular basis  $|S, m_S, I, m_I\rangle$ . Note that there is no line-to-line relation between the states listed in each column.

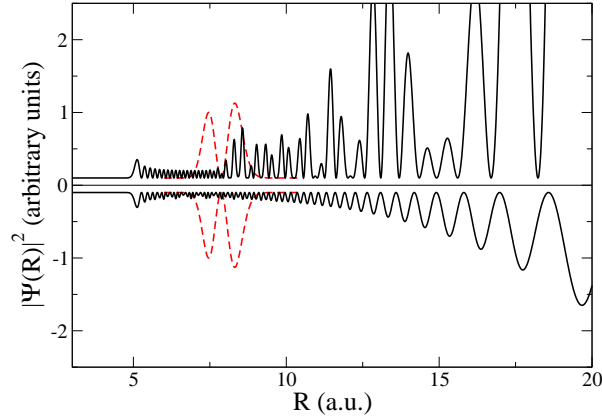


**Figure 6.** Black lines: Singlet projection of the total wave function in the coupled-channel model (upper panel), and in a single channel calculation with the singlet potential (lower panel). Probability densities for the  $v'=1$  level of the  $B^1\Pi$  state are also displayed (red dashed lines), illustrating the increased overlap due to the enhancement of the ground state wave function at the inner turning point of the triplet potential.

with the generally accepted picture of such a coupling case, the components exhibit clear irregular features resulting from the hyperfine coupling even at short internuclear distances, *i.e.* well inside the region where the atomic states decouple into triplet and singlet states. By looking at the molecular basis decomposition (right column), it is clear that the singlet component (upper panel) is so strongly coupled to the triplet component (*e.g.* third panel from the top) that they contaminate each other with their amplitude variation. In particular, the amplitude of the singlet component is strongly enhanced in the range of the triplet potential, *i.e.* from  $R = 7 \text{ a.u.}$  towards large distances, compared to the uncoupled singlet wave function (see figure 6). This “echo” of the triplet component appearing on the singlet projection of the wave function indicates that bound levels of the closed channels are energetically close to the open entrance channel. Only this situation explains the strong local perturbation of the scattering wave function. Such a hyperfine-mediated coupling between a bound level and a zero-energy continuum state is generally referred to as a Feshbach resonance.

In order to analyse how close the modeled situation is to the Feshbach resonance, we look at the squared amplitude of the collisional wave function on the closed channels as a function of the scattering energy. With the total state  $|\Psi_{\epsilon,\ell}\rangle$  of the coupled system at energy  $\epsilon$  being expressed as  $|\Psi_{\epsilon,\ell}\rangle = \sum_{\alpha=1}^4 \psi_{\epsilon,\alpha}(R) |\alpha\rangle$ , where  $\alpha$  labels the atomic hyperfine states, we define the amplitude  $P_{\alpha}(E)$  of a given hyperfine state at energy  $\epsilon$  as  $P_{\alpha}(E) = \int_0^{\infty} |\psi_{\epsilon,\alpha}(R)|^2 dR$ . This definition is only meaningful for closed channels, where  $P_{\alpha}=0$  corresponds to an unpopulated channel and  $P_{\alpha}=1$  indicates, that  $|\Psi_{\epsilon,\ell}\rangle$  is a pure bound state in channel  $\alpha$ . We plot the results for the three closed channels in figure 7. We see that indeed a resonance is present in the upper panel around  $6 \times 10^{-7} \text{ a.u.}$  (for  $\ell = 0$ ) and around  $8 \times 10^{-7} \text{ a.u.}$  (for  $\ell = 2$ ), as maxima in the amplitude of the closed-channel wave functions. Traces of these resonances are still present close to zero collision energy, where the experiment takes place. Therefore, the enhancement of the amplitude of the total scattering wave function is induced by the increased mixing arising from the presence of a broad Feshbach resonance at higher

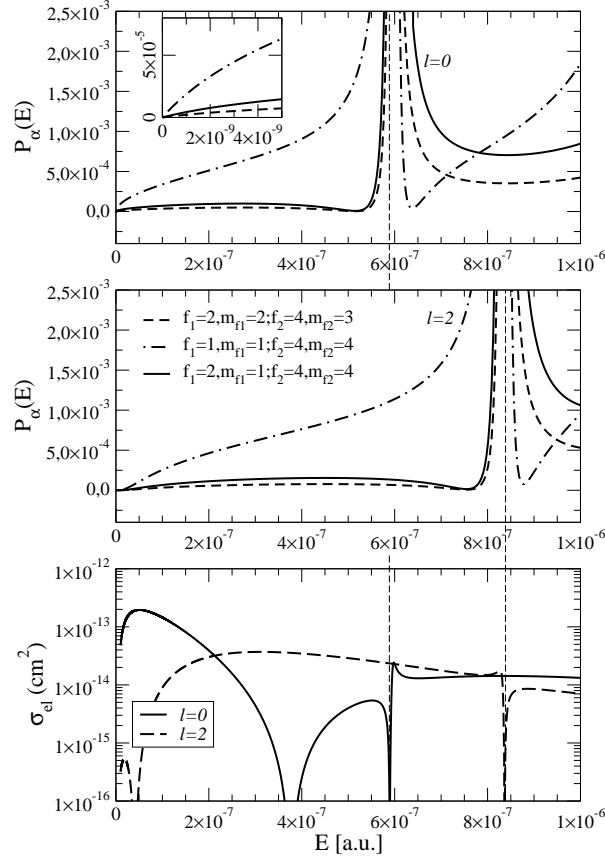


**Figure 7.** Amplitude of the  $m_F=5$  initial wave function on the three closed channels as a function of collisional energy, for  $\ell=0$  (upper panel) and  $\ell=2$  (middle panel). The inset in the upper graph shows an enlargement of the energy range for  $\ell=0$  including the collision energy of  $500 \mu\text{K}$  ( $1.6 \times 10^{-9}$  a.u.), used in all other calculations. The amplitude is given as  $P_\alpha(E)$ , the weight of the component  $\alpha$  associated to one hyperfine channel in the total wave function. Details are given in the text. Lower panel: elastic cross section for the same cases  $m_F=5$ ,  $\ell=0,2$ . The positions of Feshbach resonances are indicated by vertical dashed lines.

energy. In particular the component of the  $f_1 = 1, m_{f_1} = 1, f_2 = 4, m_{f_2} = 4$  state dominates at low energies. Note that the exact position of the resonance might not be too reliable due to uncertainties especially in the used triplet ground state potential, as discussed by the authors of reference [41]. However as we will show later, even the very weak mixing introduced by the Feshbach resonance in this calculation leads to a convincing reproduction of the experimentally observed rates, so the precise position of the resonance seems of minor relevance.

We also calculate elastic cross sections for all  $m_F$  subsystems using the log-derivative algorithm of Johnson [42]. This is another way to locate and identify possible resonances either due to the shape of potentials (shape resonances), or due to the coupling with close-by bound states (Feshbach resonances). In figure 7 (lowest panel) we show the energy-dependent elastic cross section for  $m_F=5$ . Also here,



superimposed on the regular nodal structure of the elastic cross section as one would expect it for an uncoupled case, the trace of the above mentioned resonances is visible. It is important to note that this Feshbach resonance is actually present at about the same energy in the elastic cross-sections for all values of  $m_F$ . This suggests that the singlet component of the wave function will be perturbed for all  $m_F$  in a similar way as in the presented  $m_F = 5$  case. Therefore the enhancement of the amplitude in the singlet channel should be observable for all values of  $m_F$  in a similar way and we expect that the PA rate averaged over all experimentally possible values for  $m_F$  will not strongly deviate from the value derived here for  $m_F=5$ .

#### 4.5. Comparison with experimental photoassociation rate constants

The PA rate is proportional to the transition dipole moment matrix element between the singlet component of the initial continuum state with the vibrational levels of the  $B$  state. The calculated rates assuming identical contributions from all  $m_F$  subsystems is represented in figure 8 for both coupled and uncoupled initial wave functions. As expected, both cases yield similar rates for high vibrational states, induced by a similar long-range part of the wave function. For low levels of the  $B$  state, however, the PA rate is strongly enhanced in the coupled-channel picture due to the “echo” of the triplet-like wave function on the singlet component of the wave function. It is evident that the oscillatory pattern of the experimental PA rate is well reproduced by the coupled-channel model. This oscillatory pattern arises from the variation of the overlap between the initial scattering wave function and the wave function of the excited level as the outer lobe of the latter “scans” with changing  $v'$  over the nodal structure of the former. Fair agreement between the absolute rates from experiment and theory is also found. Even though the measured values suffer from a systematic uncertainty of roughly one order of magnitude, it is obvious that the experimental observations are not compatible with the conventional picture of uncoupled singlet and triplet states at short internuclear distances.

## 5. Conclusion

By analyzing photoassociation rates of LiCs molecules in the  $B^1\Pi$  state we find that the formation rate of ground state molecules is governed by a perturbation of the ground state scattering wave function. The perturbation is caused by the existence of a Feshbach resonance at low energies, which enhances the PA rate drastically. Specifically it was shown that the singlet component of the scattering wave function, which is responsible for the efficient transfer into the  $X^1\Sigma^+$  ground state state through photoassociation and subsequent spontaneous emission, contains a strong “echo” of the triplet wave function, which allows for an efficient transfer of population from free pairs into bound molecules. As the photoassociation rate into the strongly bound levels of the excited  $B^1\Pi$  state is the rate limiting process for the formation of deeply bound ground state molecules, the perturbation leads to an increase of the formation rate by several orders of magnitude when compared to the uncoupled case.

To which extent our observations are specific to the LiCs case remains to be investigated in future experiments, but we speculate that a similar enhancement can be found in all other alkali systems. This is supported by the fact that the observed strong enhancement of the molecular formation rate is induced by the presence of a Feshbach resonance roughly 200mK (or 4GHz) above the experimental collision

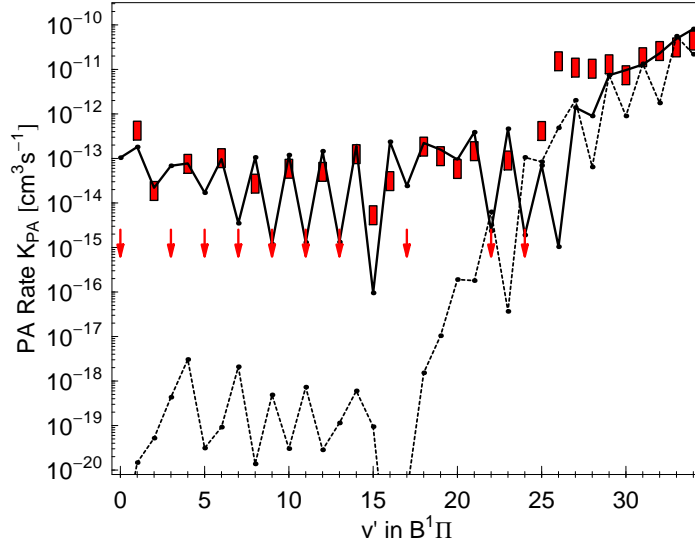


**Figure 8.** Experimental photoassociation rate constants (same data as figure 3) for the  $J'=1$  lines (filled squares), compared to the predicted values obtained for  $m_F = 5$ , in the coupled-channel picture (solid line) and in the uncoupled case (dashed line). Vibrational levels, which could not be detected experimentally, are marked by arrows indicating the detection threshold of the experiment. In the model calculation, a PA laser intensity of  $30 \text{ W/cm}^2$  and a collision energy of  $500 \mu\text{K}$  was used, corresponding to the experimental parameters. Note that the systematic error on the experimental values is about one order of magnitude, as described in Sect. 3.2.

energy, a situation which is not uncommon in alkali mixtures. We note that this kind of enhancement, or R-transfer, through coupling in the scattering wave function is complementary to other proposed and realized schemes for the transfer of weakly bound triplet molecules into ground state singlet molecules [43]. In these schemes, the “transfer” from triplet to singlet character occurs via spin-orbit mixing in the electronically excited state. In RbCs and KRb, levels in the spin-orbit coupled states  $c^3\Sigma^+$  and  $B^1\Pi$  were used to transfer weakly bound triplet molecules into absolute ground state molecules with pulsed laser fields [16, 14], while in  $\text{Cs}_2$  the coupled state  $0_u^+$  ( $b^3\Pi_u$ - $A^1\Sigma_u^+$ ) was successfully employed in a STIRAP step towards deeply bound molecules [12]. We suggest that also the wave function of most so called Feshbach molecules might exhibit an enhanced amplitude in the singlet channel at the inner turning point of the triplet potential. This would facilitate the transfer of these molecules into absolute ground state molecules via suitable excited singlet states.

The observed strong enhancement of the PA rates into the rotational component  $J'=2$  as compared to the component  $J'=1$  for low  $v$ 's is still an open question which requires further investigations. A possible explanation would be an enhancement due to a  $d$ -wave shape resonance [18], while no indication for such a resonance was found in the model presented here. Another reason for the observed ratio between rotational states could be rotational coupling with higher partial waves, which was neglected in our model. In fact, the strongly differing widths for  $J'=1$  and  $J'=2$  lines could indeed be an indication of the necessity to take into account such rotational coupling at short

distances.

## Acknowledgments

The experimental work is supported by the DFG under WE2661/6-1 in the framework of the Collaborative Research Project QuDipMol within the ESF EUROCORES EuroQUAM program. JD acknowledges partial support of the French-German University. AG is a postdoctoral fellow of the Alexander von Humboldt-Foundation. PP and RC acknowledge partial support from the U.S. Department of Energy, Office of Basic Energy Sciences.

## References

- [1] J. Doyle, B. Friedrich, R. V. Krems, and F. Masnou-Seeuws. *Eur. Phys. J. D*, 31:149, 2004.
- [2] O. Dulieu, M. Raoult, and E. Tiemann. *J. Phys. B*, 39(19), 2006. Introductory review for the special issue on Cold Molecules.
- [3] T. Zelevinsky, S. Kotochigova, and J. Ye. *Phys. Rev. Lett.*, 100:043201, 2008.
- [4] T. V. Tscherbul and R. V. Krems. *Phys. Rev. Lett.*, 97:083201, 2006.
- [5] A. Micheli, G. K. Brennen, and P. Zoller. *Nature Physics*, 2:341, 2006.
- [6] G. Pupillo, A. Griessner, A. Micheli, M. Ortner, D.-W. Wang, and P. Zoller. *Phys. Rev. Lett.*, 100:050402, 2008.
- [7] D. DeMille. *Phys. Rev. Lett.*, 88:067901, 2002.
- [8] S. F. Yelin, K. Kirby, and R. Côté. *Phys. Rev. A*, 74:050301, 2006.
- [9] P. Rabl, D. DeMille, J. M. Doyle, M. D. Lukin, R. J. Schoellkopf, and P. Zoller. *Phys. Rev. Lett.*, 97:033003, 2006.
- [10] E. Charron, P. Milman, A. Keller, and O. Atabek. *Phys. Rev. A*, 75:033414, 2007.
- [11] F. Lang, K. Winkler, C. Strauss, R. Grimm, and J. Hecker Denschlag. *Phys. Rev. Lett.*, 101:133005, 2008.
- [12] J. G. Danzl, E. Haller, M. Gustavsson, M. J. Mark, R. Hart, N. Bouloufa, O. Dulieu, H. Ritsch, and H.-C. Nägerl. *Science*, 321:1062, 2008. H.-C. Nägerl *private communication*.
- [13] J. G. Danzl, M. J. Mark, E. Haller, M. Gustavsson, N. Bouloufa, O. Dulieu, H. Ritsch, R. Hart, and H.-C. Naegerl. *arXiv:0811.2374v1 [cond-mat.other]*, 2008.
- [14] K.-K. Ni, S. Ospelkaus, M. H. G. de Miranda, A. Pe'er, B. Neyenhuis, J. J. Zirbel, S. Kotochigova, P. S. Julienne, D. S. Jin, and J. Ye. *Science*, 322:231, 2008.
- [15] A. N. Nikolov, J. R. Ensher, E. E. Eyler, H. Wang, W. C. Stwalley, and P. L. Gould. *Phys. Rev. Lett.*, 84:246, 2000.
- [16] J. M. Sage, S. Sainis, T. Bergeman, and D. DeMille. *Phys. Rev. Lett.*, 94:203001, 2005.
- [17] M. Viteau, A. Chotia, M. Allegrini, N. Bouloufa, O. Dulieu, D. Comparat, and P. Pillet. *Science*, 321:232, 2008.
- [18] J. Deiglmayr, A. Grochola, M. Repp, K. Mörtlbauer, C. Glück, J. Lange, O. Dulieu, R. Wester, and M. Weidemüller. *Phys. Rev. Lett.*, 101:133004, 2008.
- [19] M. Aymar and O. Dulieu. *J. Chem. Phys.*, 122:204302, 2005.
- [20] J. Deiglmayr, M. Repp, A. Grochola, K. Mörtlbauer, C. Glück, J. Lange, O. Dulieu, R. Wester, and M. Weidemüller. *Accepted for publication in Faraday Discussions* 142, 2009. Also at arXiv:0812.1002v1.
- [21] P. Pellegrini, M. Gacesa, and R. Côté. *Phys. Rev. Lett.*, 101:053201, 2008.
- [22] S. D. Kraft, J. Mikosch, P. Staunum, J. Deiglmayr, J. Lange, A. Fioretti, R. Wester, and M. Weidemüller. *Appl. Phys. B*, 89:453, 2007.
- [23] W. Ketterle, K. B. Davis, M. A. Joffe, A. Martin, and D. E. Pritchard. *Phys. Rev. Lett.*, 70:2253, 1993.
- [24] K. M. Jones, P. D. Lett, E. Tiesinga, and P. S. Julienne. *Phys. Rev. A*, 61:012501, 1999.
- [25] H. R. Thorsheim, J. Weiner, and P. S. Julienne. *Phys. Rev. Lett.*, 58:2420, 1987.
- [26] K. M. Jones, E. Tiesinga, P. D. Lett, and P. S. Julienne. *Rev. Mod. Phys.*, 78:483, 2006.
- [27] R. Côté and A. Dalgarno. *Chem. Phys. Lett.*, 279:50, 1997.

- [28] A. Stein, A. Pashov, P.F. Staunum, H. Knöckel, and E. Tiemann. *Eur. Phys. J. D*, 48:177, 2008.
- [29] D. A. Verner, G. J. Ferland, K. T. Korista, and D. G. Yakovlev. *Astrophys. J.*, 465:487, 1996.
- [30] G. W. Fraser. *Int. J. Mass Spect.*, 215:13, 2002.
- [31] C. Drag, B. Laburthe Tolra, O. Dulieu, D. Comparat, M. Vatasescu, S. Boussen, S. Guibal, A. Crubellier, and P. Pillet. *IEEE J. Quantum Electron.*, 36:1378, 2000.
- [32] R. Wester, S.D. Kraft, M. Mudrich, M.U. Staudt, J. Lange, N. Vanhaecke, O. Dulieu, and M. Weidemüller. *Appl. Phys. B*, 79:993, 2004.
- [33] M. W. Mancini, G. D. Telles, A. R. L. Caires, V. S. Bagnato, and L. G. Marcassa. *Phys. Rev. Lett.*, 92:133203, 2004.
- [34] S. Azizi, M. Aymar, and O. Dulieu. *Eur. J. Phys. D*, 31:195, 2004.
- [35] R. Napolitano, J. Weiner, C. J. Williams, and P. S. Julienne. *Phys. Rev. Lett.*, 73:1352, 1994.
- [36] A. Grochola, A. Pashov, J. Deiglmayr, M. Repp, E. Tiemann, R. Wester, and M. Weidemüller. *In preparation*.
- [37] T. Bergeman, P. S. Julienne, C. J. Williams, E. Tiesinga, M. R. Manaa, H. Wang, P. L. Gould, and W. C. Stwalley. *J. Chem. Phys.*, 117:7491, 2002.
- [38] Th. Udem, J. Reichert, R. Holzwarth, and T. W. Hänsch. *Phys. Rev. Lett.*, 82:3568, 1999.
- [39] Th. Udem, J. Reichert, T. W. Hänsch, and M. Kourogi. *Phys. Rev. A*, 62:031801, 2000.
- [40] V. Kokoouline, O. Dulieu, R. Kosloff, and F. Masnou-Seeuws. *J. Chem. Phys.*, 110:9865, 1999.
- [41] P. Staunum, A. Pashov, H. Knöckel, and E. Tiemann. *Phys. Rev. A*, 75:042513, 2007.
- [42] B.R. Johnson. *J. Comp. Phys.*, 13:445, 1973.
- [43] W.C. Stwalley. *Eur. Phys. J. D*, 31:221, 2004.